AFRL-AFOSR-UK-TR-2011-0060

Experimental Study of Auto-Ignition Phenomena in Swirl-Stabilized LPP Flames in Gas Turbine Model Combustors using kHz Framerate OH-PLIF and Stereo-PIV

Isaac G. Boxx

Deutsches Zentrum fur Luft- und Raumfahrt
Institut fur Verbrennungstechnik
Pfaffenwaldring 38-40
Stuttgart, Germany 70569

EOARD GRANT 10-3052

Report Date: January 2012

Final Report for 01 July 2010 to 01 January 2012

Air Force Research Laboratory
Air Force Office of Scientific Research
European Office of Aerospace Research and Development
Unit 4515 Box 14, APO AE 09421

REPORT DOCUMENTATION PAGE

Form Approved OMB No. 0704-0188

1. REPORT DATE *(DD-MM-YYYY)*	2. REPORT TYPE	3. DATES COVERED *(From – To)*
23-01-2012	Final Report	1 July 2010 – 1 January 2012

4. TITLE AND SUBTITLE

Experimental Study of Auto-Ignition Phenomena in Swirl-Stabilized LPP Flames in Gas Turbine Model Combustors using kHz Framerate OH-PLIF and Stereo-PIV

5a. CONTRACT NUMBER

FA8655-10-1-3052

5b. GRANT NUMBER

Grant 10-3052

5c. PROGRAM ELEMENT NUMBER

6. AUTHOR(S)

Dr. Isaac G. Boxx

5d. PROJECT NUMBER

5d. TASK NUMBER

5e. WORK UNIT NUMBER

7. PERFORMING ORGANIZATION NAME(S) AND ADDRESS(ES)

Deutsches Zentrum fur Luft- und Raumfahrt
Pfaffenwaldring 38-40
Stuttgart, Germany 70569

8. PERFORMING ORGANIZATION REPORT NUMBER

N/A

9. SPONSORING/MONITORING AGENCY NAME(S) AND ADDRESS(ES)

EOARD
Unit 4515 BOX 14
APO AE 09421

10. SPONSOR/MONITOR'S ACRONYM(S)

AFRL/AFOSR/RSW (EOARD)

11. SPONSOR/MONITOR'S REPORT NUMBER(S)

AFRL-AFOSR-UK-TR-2011-0060

12. DISTRIBUTION/AVAILABILITY STATEMENT

Approved for public release; distribution is unlimited. (approval given by local Public Affairs Office)

13. SUPPLEMENTARY NOTES

14. ABSTRACT

Long-duration, kHz-framerate OH-PLIF measurements were analyzed to determine the physical mechanism responsible for a previously observed phenomenon wherein isolated pockets of high OH-concentration fluid suddenly appear in regions of unburned gas away from the contiguous flame zone in a gas turbine model combustor. Prior research on the burners indicate these isolated flame-kernels may result either from auto-ignition of hot, unburned reactants upstream of the primary flame or from transport of reacting fluid into the field of view from beyond the imaging plane. An image-processing routine was developed to autonomously identify and statistically characterize these flame-kernels. Phase sorting of the kernel centroids with respect to the dominant fluid-dynamic structure of the combustors (a helical precessing vortex core or thermo-acoustically forced shear-layer vortices) indicate through-plane transport of reacting fluid best explains their sudden appearance the PLIF images. The concentration of flame-kernel events around the periphery of the mean location of the precessing vortex core (PVC) indicates they are likely the result of wrinkling and break-up of the primary flame sheet associated with the passage of the PVC as it circumscribes the burner centerline. The prevailing through-plane velocity of the swirling flow-field transports these fragments into the imaging plane of the OH-PLIF system. The lack of flame-kernel events near the center of the PVC, where conditions are more conducive to auto-ignition (lower strain, longer fluid dynamic residence time), indicates auto-ignition is not a viable explanation for these flame-kernels in a majority of cases. The lack of flame-kernel centroid variation in the case of the TM-Burner 'Quiet flame' (which has no PVC) further supports this explanation.

15. SUBJECT TERMS

EOARD, Experimental, turbine engines, Combustion Modeling

16. SECURITY CLASSIFICATION OF:			17. LIMITATION OF ABSTRACT	18, NUMBER OF PAGES	19a. NAME OF RESPONSIBLE PERSON
a. REPORT	b. ABSTRACT	c. THIS PAGE			Gregg Abate
UNCLAS	UNCLAS	UNCLAS	SAR	28	19b. TELEPHONE NUMBER *(Include area code)* +44 (0)1895 616021

Final Report

FA8655-10-1-3052

Experimental Study of Auto-Ignition Phenomena in Swirl-Stabilized LPP Flames in Gas Turbine Model Combustors using kHz Framerate OH-PLIF and Stereo-PIV

Dr. Isaac Boxx

Deutsches Zentrum für Luft- und Raumfahrt e.V.
Institut für Verbrennungstechnik
Pfaffenwaldring 38-40
D-70569 Stuttgart

isaac.boxx@dlr.de

Isolated Flame Kernels in Swirl-Stabilized Lean Partially Premixed Flames: Auto-ignition or Flame Dynamics in Third Dimension

Introduction

The gas turbine (GT) engine is a critical enabling technology for modern aviation and large-scale power generation. Their extensive application, however, has made pollutant emissions from such engines a point of environmental concern, and in recent years, a major goal in GT development has been a significant reduction in emissions of oxides of Nitrogen (NO_x). This goal has lead to considerable interest in the concept of lean premixed- and partially-premixed (LPP) combustion. LPP combustion can produce a quite homogeneous temperature distribution at the turbine inlet and thus reduced thermal load so the high peak temperatures of near-stoichiometric conditions responsible for NO_x production are avoided [Correa, (1998); Lefebvre, (1999)]. Unfortunately, stabilization of LPP flames is particularly challenging due to their susceptibility to thermo-acoustic instability and blow-out.

The physical mechanism governing flame stabilization and thermo-acoustic pulsation in swirled LPP combustors depends on a complex, interdependent coupling of multiple thermo-physical, chemical and fluid-dynamic parameters. The turbulence-chemistry interaction occurs over a wide range of spatial and temporal scales and is strongly coupled to specific, system-dependent boundary conditions. Despite ongoing advances in theoretical models, computational power and experimental methods, there remains a lack of highly accurate, robust and reliable predictive tools for the design and optimization of combustion technology (Barlow, 2007). This is due in part to the fact that practical design and predictive analysis codes for turbulent combustion systems necessarily rely on simplified models and assumptions to make the problem computationally tractable. The accuracy and reliability of these models and assumptions depend on a thorough fundamental understanding of the processes responsible for specific turbulence-chemistry interactions.

With this in mind, there has been a sustained effort in recent years to acquire high spatial- and temporal-resolution measurements of multiple combustion parameters in well-characterized, laboratory-scale combustors. The resulting data is then used to test and validate the simplifying assumptions used in predictive analysis and design codes. This effort has relied extensively on point- and planar-laser diagnostic techniques to measure velocity, major and minor species concentrations and - their spatial distributions - and temperature. Derivative quantities such strain rate, vorticity and scalar dissipation have also been measured. Such measurements, particularly those used in combination with acoustic data to achieve phase-averaged measurements over the thermoacoustic oscillation, have yielded extensive new insight into the physics of LPP combustion in GT engines. These efforts however, have met limited success when applied to the study of transient and spatio-temporally unpredictable phenomena such as local extinction, blow-off and auto-ignition. This stems from the relatively low (≈ 1 - 10 Hz) repetition rates of standard planar imaging techniques such as particle image velocimetry (PIV) and planar laser-induced fluorescence (PLIF), which prevents one from tracking the temporal development of individual flow structures and their interaction with the flame front.

The recent development of planar measurement systems with multi-kHz acquisition rates and measurement periods of one second or more have made it possible, for the first time, to statistically characterize spatiotemporally unpredictable phenomena occurring in turbulent flames. Böhm et al. (2008), for example, used simultaneous highspeed-PIV and PLIF to study vortex-flame interactions leading to local extinction of a turbulent, opposed-jet flame. Steinberg et al. (2010) used similar diagnostics to study flame-hole re-ignition in a turbulent jet flame. Stöhr et al. (2010) used highspeed stereo-PIV, OH-PLIF and OH* chemiluminescence imaging to study flame blow-out in a gas turbine model combustor.

In a series of studies by Boxx et al. (2009a, 2009b, 2010a, 2010b), multi-kHz framerate stereoscopic-PIV and OH-PLIF were applied simultaneously to study LPP swirl flames in a series of gas turbine model combustors. These measurements have yielded a wealth of new insight into the flowfield and turbulence-chemistry interaction of these flames. They showed the existence of a helical precessing vortex core in the combustor, the effect of vortex-flame

interaction in the recirculation zone and the impact of thermoacoustic pulsation on the flowfield and flame dynamics. The data also raised unexpected new questions. Of particular interest in the measurements were incidents wherein isolated pockets of OH were observed to suddenly appear in regions of unburned gas upstream of the contiguous reaction zone. We refer to these incidents as 'flame-kernel events'. Flame-kernel events likely arise from one of two physical mechanisms: through-plane convection and propagation of the flame, or auto-ignition of unburned gas within the imaging-plane. A close examination of point measurements of mixture fraction and temperature acquired in an earlier study via spontaneous Raman scattering in the same burner under identical conditions indicates that auto-ignition may be a viable explanation in some instances. Comparison of these OH regions to the corresponding instantaneous through-plane fluid velocity (measured via stereo-PIV) indicates that through-plane convection is not a universally viable explanation. As the measuring system only identifies the presence of OH and not its source (i.e. transport vs. production), it is impossible to determine conclusively from the PLIF data which explanation is correct for a given instance. The goal of the present study was to statistically characterize the flame-kernel events seen in the Boxx et al. studies and to determine the most probable physical mechanism responsible for them.

Experiments

Data from measurements in two swirl-stabilized burners was analyzed in this study: the DLR Dual-Swirl (DS) Burner and the Turbomeca Gas Turbine Model Combustor (TM-Burner). Both burners have been extensively characterized and are well-described in a series of recent publications (Giezendanner-Thoben et al. 2003, 2005a, 2005b, 2005c, Boxx et al. 2010a, Duan et al. 2005, Meier et al. 2007, Boxx et al. 2010b). Therefore, only a brief overview of each is presented here.

Dual-Swirl Burner

The DS-Burner consists of two parts: a central nozzle for the introduction of methane and swirled air into the combustor and an optically accessible combustion chamber. In this burner dry, room temperature air enters the combustion chamber through a 15 mm diameter central nozzle. This nozzle is surrounded by a concentric annular nozzle (i.d. 17

mm, o.d. 25 mm contoured to an o.d. of 40 mm). Air enters each nozzle through a set of radial swirl vanes fed from a common plenum. In this study, co-swirl was used. Non-swirling CH_4 enters the chamber via a ring of 72 channels (0.5 mm x 0.5 mm) located between the two air nozzles. The exit planes of the fuel and central air nozzle stand 4.5 mm below the exit plane of the outer air nozzle. The combustion chamber has a square cross-section measuring 85 mm x 85 mm and stands 110 mm tall. The walls of the chamber are quartz plates held at the corners with Inconel® alloy posts (dia. 10 mm). The chamber is capped with a steel plate with a central exhaust tube (dia. 40 mm, length 50 mm) over a conical contraction.

The flame studied in this work corresponds to that described as "Flame B' in the work of Weigand et al. [2006]. It has a 10kW thermal load, corresponding to 12.3 g/min of CH_4 and 281 g/min of air. It has swirl number of 0.55. Prior studies have shown (Giezendanner et al. 2003, 2005) that this flame displays a strong thermoacoustic pulsation at 308 Hz and its flow-field is dominated by a helical precessing vortex core or (PVC) that circumscribes the central axis of the burner at approximately 515 Hz (Boxx et al. 2010a).

TM-Burner

The TM Burner is a laboratory-scale swirl burner based on an industrial design by Turbomeca S.A. It is operated with a lean CH_4 / air flame at atmospheric pressure. Dry air at room temperature is fed via a 78 mm diameter plenum into a central nozzle through 12 radial swirl-vanes. Fuel is injected directly into the swirler through twelve 1-mm diameter holes. The exit of the burner nozzle is 27.85 mm in diameter and has a rounded, conical centerbody. The nozzle exits into a combustion chamber identical to that used by the DS-Burner. The injection of gaseous methane at the radial swirl vanes results in significant, (albeit imperfect) premixing of the fuel and air prior to its entry into the combustion chamber.

Data from two flame conditions in this burner were analysed in this study: a 25 kW flame with strong self-excited thermo-acoustic pulsations (the '*noisy flame*'), and a 30 kW flame that burns stably and without strong thermo-acoustic pulsation (the '*quiet flame*'). Both flames were operated with 740 g/min of air. The *noisy* and *quiet* flames had equivalence ratios of 0.73 and 0.83 (corresponding to 30 and 36 g/min CH_4), respectively. These run

conditions were chosen to replicate those studied by Meier et al. [2007], designated Flame 1 and Flame 2a, respectively. The same flames were further characterized in Boxx et al. [2010].

Planar Imaging Diagnostics

The data analyzed in this study was acquired using the DLR highspeed planar measurement system (Boxx et al. 2009a, 2009b, 2010a, 2010b). This system consists of a planar laser induced fluorescence (PLIF) system for the imaging of the hydroxyl (OH) radical and a stereoscopic particle image velocimetry (PIV) for the measurement of the 3-component velocity field in a plane. The system was used to acquire simultaneous planar measurements of the OH distribution and 3-component velocity field in a plane at 5- and 10 kHz repetition rates for flames in the DS- and TM-Burner, respectively. Measurement durations for each were approximately 0.8 seconds. The high frame-rate and relatively long measurement duration of the system enable the acquisition of time-resolved measurements of the flowfield-flame interaction over several hundred thermo-acoustic cycles. The spatial resolution of the PIV was 1mm in the DS-Burner measurements and 1.1mm in the TM-Burner. The OH-PLIF measurements in the DS-Burner spanned the width of the combustor (85mm) and extended 40mm downstream of the nozzle exit. For the measurements made in the TM-Burner, the PLIF imaging region spanned approximately 50mm (wide) × 45mm (high) and covered slightly more area to the right of the burner centerline than the left.

Image Processing

The objective of this study was to identify the physical mechanism responsible for the flame-kernel events described earlier. In particular, the objective was to determine the viability of the hypothesis that these OH-concentrations result from auto-ignition of high-temperature fuel-air mixtures away from the primary reaction zone. To accomplish this, image processing tools were developed to automate the identification and statistical characterization of these events. These tools are described below.

Flame Kernel Identification

Figure 2 shows a typical OH-PLIF image acquired in the DS-Burner. The imaging region covers the width of the combustion chamber (85 mm) and extends approximately 40 mm downstream of the nozzle. In this image, the regions without OH (dark) are believed to represent gas at low-to-medium temperatures (T < 1500 K), e.g. fresh fuel/air mixtures, possibly with some admixture of burned gas. From Raman measurements in the same flame, it is known that there is significant mixing of exhaust gas with fresh gas near the nozzle and the gas mixture can cover a wide temperature range (300 - 1500 K). The light-grey regions (i.e. those with moderate-to-high OH signal levels) within the IRZ and ORZ consist primarily of gas at high temperature (> 1500 K). The brightest regions of the image are indicative of super-equilibrium concentrations of OH. Sadanandan, et al. [2008] showed that, for this flame, the largest magnitude OH-gradients result from super-equilibrium concentrations of OH and are thus representative of the reaction zone of the flame. Lower magnitude OH-gradients downstream of the contiguous reaction zone tend to be indicative of mixing and diffusion of OH as it moves away from the reaction zones.

It is apparent from Figure 2 that most of the measurable concentrations of OH occur in a contiguous region. This region is centered in the inner recirculation zone (IRZ) of the burner, but extends to the walls of the combustion chamber and even into the outer recirculation zone (ORZ). At the periphery of this largely contiguous region of OH is a clearly identifiable interface between burned and unburned gas. The large OH-gradient magnitude associated with this interface indicates a largely intact flame sheet in the burner. Also apparent in Figure 2 are several isolated regions of OH upstream of the contiguous flame front. These appear in the region of unburned gas several millimetres downstream and to the right of the nozzle exit. Although it is not apparent in single-frame PLIF image such as this, these OH-concentrations represent flame-kernel events.

Flame Kernel Extraction

The extraction of flame kernel information from the OH-PLIF data occurred in two stages: image filtering / pre-processing and flame kernel identification. The goal of the first step was to reduce the raw OH-PLIF images to a format wherein isolated flame kernels are readily

identifiable by automated checks. The goal of the second step is to apply a series of checks based on physical criteria to identify newly-appearing flame kernels.

Image Processing

The first step of reducing the raw OH-PLIF images to usable data was the correction for physical parameters such as laser sheet uniformity and camera sensitivity. Correction of the OH-PLIF images for imaging system sensitivity was accomplished by acquiring a series of 1000 images of a uniform illumination lamp. These images were acquired with the same optical configuration and intensifier gain settings used the PLIF imaging experiments. The ensemble average of these images was then used to correct each PLIF image for camera / intensifier sensitivity. Correction for non-uniformity of the laser-sheet profile was accomplished by acquiring 1000 images of acetone vapor doped into the combustion chamber of the burner. The ensemble-average of these images was similarly used to correct individual PLIF images for laser sheet non-uniformity. The resulting images were then spatially calibrated based on a two-plane calibration target. This calibration eliminates spatial distortions of the imaging objective. It also links the spatial coordinates of the corrected PLIF image to that of the combustor and the simultaneously acquired PIV measurement data.

The corrected images were then cropped to show only that region of the combustor illuminated by the laser sheet. The cropped images are then binned (2 × 2) to halve their original size to increase the signal-to-noise ratio and a low-pass, 5 × 5 median filter was applied to smooth the images. The resulting images were binarized based on a user-defined intensity threshold. This threshold was determined empirically, based on how robustly it captures the OH / unburned-gas interface, as well as the low-intensity regions of OH in the combustion products further downstream. The binary images were then expanded back to their original size for Phase-2 post-processing.

Step two of the flame kernel detection algorithm was based on a series of checks of the binary images to identify newly-appearing flame kernels. The first of these checks is

designed to eliminate the primary flame front of visible in the image. Using binary image labeling with 8-point connectivity, each contiguous region of OH in the measurement was identified. Prior knowledge of the flames under study indicates the largest contiguous region of OH in the PLIF images corresponds to the primary flame zone and post-combustion products. The largest labeled region in the binary image was thus assumed to correspond to the primary flame zone and was eliminated.

Next, any regions identified as adjacent to the combustor windows were eliminated. This is based on the assumption that heat-loss there makes auto-ignition exceedingly unlikely for these flames. Regions of OH adjacent to the exit plane or the upper edge of the PLIF laser-sheet were also eliminated. At the exit plane, it is impossible to distinguish the in-plane extent of OH-regions due to cut-off of optical access at the burner nozzle. Similarly, the cut-off height of the PLIF laser sheet makes it impossible to rigorously determine the in-plane spatial characteristics of the OH-regions it transects.

What remains after these checks are binary images that may (or may not) contain one or more flame kernels. Only those OH concentrations which appear for the first time in the frame represent flame kernel events. Therefore, binary image labeling was used to identify each region of OH. Each region was then individually checked for overlap with the (complete) binary OH-image from the previous measurement frame. Those showing overlap are assumed to be associated with the OH-zone of the frame before and thus eliminated from further consideration. Kernels with no overlap of OH from the previous frame are thus newly-appearing OH kernels.

Figure 3 shows a series of PLIF images after each stage of the image processing. The first row shows three corrected OH-PLIF images. The second row shows the resulting binary images. The third row shows newly-appearing OH concentrations identified in step two of the kernel identification algorithm. This figure shows both the robustness of the algorithm and its limitations. The robustness shows in its ability to both eliminate the primary OH-region and those present in the prior images. Its limitation is sensitivity to the choice of intensity threshold used to binarize the images. Although super-equilibrium concentrations of OH

present in the reaction zone result in a clearly identifiable interface between burned and unburned gases near the nozzle exit, the lower (equilibrium-level) OH concentrations in post-combustion products further downstream result in sensitivity to the intensity threshold. As Figure 3 shows, however, the region affected by this threshold-sensitivity is highly localized (about the burner centerline and approximately 30mm downstream) and in a region known to consist almost entirely of post-combustion products. Thus the effect is easily identifiable in the resulting statistics and can therefore be neglected in subsequent analysis.

Kernel Characterization

Application of the flame-kernel event detection routines described above results in series of binarized images similar to those shown in Row 3 of Figure 3. An automated binary image processing routine was written to scan through the processed images to extract the number of kernels in each frame, their centroid locations and area. The centroid locations were used to determine the local velocity-field characteristics at the flame-kernel events. These data form the basis of the statistics presented below.

It is important to also note the limitations of the resulting statistics. Due to experimental considerations, the field of view of the PIV measurements was significantly smaller than that of the PLIF data in the measurements made in the DS-Burner. Therefore, a significant fraction of flame-kernel events occur in regions where no velocity data was available. Statistics relating to local velocity field characteristics are therefore limited to those regions within the measurement window. For the case of the TM-Burner, there is almost complete overlap of the PIV and PLIF measurement regions. The field of view, however, does not span the full width of the combustor. The measurement area for the TM-Burner was also aligned more to the right side of the burner, biasing the through-plane velocity field statistics toward higher positive values.

Results and Discussion

Prior research indicates the presence of a helical precessing vortex core (PVC) in the flowfield of the DS-Burner and in the 'Noisy Flame' test condition studied in the TM-Burner. Proper orthogonal decomposition (POD) analysis has shown the PVC to be a dominant fluid-dynamic structure in these flames. It resides primarily along the shear-layer between the relatively high-velocity jet of incoming reactants and the inner recirculation zone (IRZ) of the combustor. The passage of the PVC through the combustor flowfield is linked to the phase of the multiplicative constant of the dominant eigenmode of the flowfield. Given its dominant role in combustor dynamics, it likely plays some role in the physical mechanism responsible for flame kernel events. As such, flame-kernel statistics were sorted into eight bins according to the phase of the PVC, as identified in the multiplicative constant of the first mode of the POD.

Figure 4 shows the phase-sorted probability distribution of Flame-Kernel events with the DS-Burner. Each plot represents approximately 510 measurement frames ($1/8^{th}$ of a 4096-measurement time series) and contains between 848 and 1030 flame kernel events. Figure 4 shows that the spatial distribution of flame kernel events is quite localized and is centered in the region of the shear-layer between incoming reactants and the inner recirculation zone. This is to be expected, as prior work has shown conclusively that the reaction zone of the flame resides primarily in the shear-layer.

Figure 4 shows the spatial distribution of flame kernel events varies with the phase of the helical PVC. At Phase 1, the distribution peaks approximately 15mm to the right and 8mm above the origin. A weaker, secondary peak in the distribution is seen on the left side of the combustor. The small cluster of flame kernel events appearing at the downstream centerline stems from the aforementioned threshold sensitivity in the kernel identification algorithm. Over phases 2 and 3, we see the peak on the right hand side dissipate and the peak to the left increase in magnitude. At phase 4, the peak on the left side begins to dissipate. This dissipation continues over phases 5 through 8. At the same time, the peak to the right side grows in magnitude. It is also important to note that axial and radial coordinates of peak flame-kernel concentration on the left and the right side of the combustor also vary with the phase of the PVC. This is consistent with the flame kernel distribution being coupled with

PVC precession, as the PVC itself is (instantaneously) asymmetric about the burner centerline.

Figure 5 shows the phase-averaged velocity field data for the same flame. The color contours represent velocity magnitude. The white lines overlaid are stream-traces. Figure 5 illustrates the effect of the PVC on combustor dynamics. At phase 1 we see a vortex centered approximately 6mm to the left and 4mm downstream of the nozzle. This vortex lies in the shear-layer between the incoming reactants and the inner recirculation zone (IRZ). A second vortex (centered 15mm to the left and 28mm downstream) is also present. A third vortex is observed approximately 9mm to the right of centerline and approximately 13mm downstream of the exit. These three vortices represent planar cuts through the helical PVC, which spirals up around the burner centerline, growing in size with downstream distance. Although the field of view of the PIV measurement is insufficient to track these vortices over the entire combustor, it is clear they grow in size and move downstream over a cycle of PVC precession. At phase 4, we see what appears to be a new vortex propagating up into the measurement plane from the exit of the combustor. At phase 5, this vortex is fully visible on the right side and the flow-field essentially mirrors that seen at phase 1. This is to be expected, as prior research has shown this phase of the PVC represents its precession about the burner centerline.

The effect of the PVC on the shear-layer between incoming reactants and the IRZ of the combustor is apparent in the velocity magnitude contours plotted in Figure 5. The PVC induces significant distortion of the shear-layer as it precesses through the combustor. As much of the reaction zone in this flame resides in the shear-layer, this PVC-induced distortion can be expected to significantly impact flame sheet wrinkling and curvature. Indeed, evidence of this has been reported in prior studies on the flame (Steinberg et al., 2011). Figure 6 shows the same phase-averaged data overlaid on the Vz-component of velocity. It is clear from this figure that the precession of the PVC does not induce a major disruption in the through-plane component of velocity.

Comparison of Figures 4, 5 and 6 reveals a number of clues as to the physical mechanism responsible for the flame kernel events. It was noted above that the concentration of flame kernel events at phase 1 occurs at (x,y) ≈ (15mm, 8mm). Inspection of the phase-averaged velocity field data in Figure 5 shows that this point stands at the outer periphery of one of the vortices identified as representing the PVC. Indeed, the peak concentration of flame kernel events at this phase of the PVC precession is found almost directly between the center of the PVC and the high-velocity jet of incoming reactants. The high strain and strong mixture fraction variations here are far less conducive to auto-ignition than just a few millimeters away at the core of the precessing vortex. The remaining plots in Figures 4-6 reveal similar correlation for each phase-angle. At phase 6, for example, the peak flame kernel concentration is observed at (x,y) ≈ (9mm, 7mm). It is clear from Figure 5 that this point is also at the outer periphery of the PVC and within the high-velocity shear layer between incoming reactants and the IRZ. No significant difference in the through-plane velocity field is observed at this location at Phase 6 in Figure 6.

The concentration of flame kernel events in the shear-layer around the outer-periphery of the mean PVC location indicates the kernels appear most frequently in a region not conducive to auto-ignition. Rather, they occur in a region of the flow highly conducive to flame wrinkling and strain-induced local extinction. The lack of corresponding fluctuation in the through-plane (Vz) velocity field indicates the flame-kernel appearance is unlikely an effect of the precession of the PVC dragging more flame sheet into the measurement volume as it precesses through the combustor. Flame-kernel events are therefore likely the result of increased flame-sheet wrinkling and breakup induced by the passage of the PVC through the combustor. Fragments or tendrils of the flame sheet resulting from this interaction are transported into the PLIF imaging plane by the prevailing through-plane velocity of the swirling flow in what we identify as flame-kernel events.

Figure 7 shows the phase-sorted probability distribution of flame-kernel events for the ‘Noisy flame’ condition measured in the TM-Burner. Despite the fact that the OH-PLIF images in this case do not span the entire width of the combustor, a similar correlation between the spatial distribution of flame kernel events and the passage of the PVC is

observed. In this case, at Phase 1 the distribution of flame-kernel events occurring to the right of centerline peaks at (x,y) ≈ (18mm, 25mm). Figure 8 shows the corresponding phase-averaged velocity fields. Here again, we see the peak concentration of flame kernel events occurs in the shear-layer region at the outer periphery of the vortex centered at (x,y) ≈ (12mm, 20mm). The spatial distribution of flame-kernel events is considerably broader in this case compared to that seen in the DS-Burner. This is consistent with the considerably larger area over which the vortex / shear-layer interaction takes place in this flame. Here again, we see little evidence of a significant disruption of the through-plane velocity field. Inspection of the flame-kernel event distributions at each subsequent phase shows they consistently peak in the shear-layer region at the outer periphery of the PVC. The similarity in peak flame-kernel event concentration despite significant differences in fuel-air mixing characteristics between the two burners is also consistent with a fluid-dynamic mechanism (i.e. flame-wrinkling and breakup induced by the PVC traversing the shear-layer) rather than a thermo-chemical (i.e. auto-ignition) mechanism being responsible for the flame kernel events.

Figure 9 shows the distribution of flame-kernel events measured in the 'Quiet flame' case studied in the TM-Burner, phase-sorted according to the dominant velocity field eigenmode. Consistent with the results seen for the 'Noisy flame' case and in the DS-Burner, flame-kernel events are concentrated in the shear-layer between incoming reactants and the IRZ. Indeed, the peak concentration of flame-kernel events is higher in this case than in either of the other two. The results are unique, however, in that the peak concentration remains virtually unchanged when sorted with respect to the dominant eigenmode of the velocity field. The axial location of peak flame-kernel event concentration varies with the phase of the dominant eigenmode but its magnitude remains largely constant. Figure 10 shows the corresponding phase-averaged velocity fields for this case. Consistent with the previous two cases, peak concentration of flame-kernel events occurs in the shear-layer at the periphery of a large vortex.

Prior research has shown (Boxx et al. 2010b) that no PVC exists in the combustor flow-field for the 'Quiet Flame' case in the TM-Burner. The dominant velocity-field eigenmode is

representative of a resonant acoustic mode of the combustor. The periodic fluctuation seen in this POD mode is linked to the (very weak) self-excited thermoacoustic pulsation of this flame. The vortices seen in the phase-averaged velocity field in this case represent shear-layer vortices shed at the combustor exit that propagate up through the flow. A weak, self-excited thermo-acoustic pulsation at this resonant frequency helps drive the propagation of these vortices as they move through the shear-layer.

The results shown in Figures 9 and 10 are consistent with vortex-induced flame wrinkling and break-up being the dominant mechanism responsible for flame-kernel events observed in this combustor. In this case however, it is shear-layer vortices that induce this wrinkling and break-up rather than a PVC. The absence of a PVC for this flame condition results in more circumferentially uniform shear-layer vortices. This explains the lack of phase-dependence in the peak concentration of in-plane flame-kernel events. The axial variation of peak flame-kernel concentration is consistent with axial velocity fluctuations induced with thermo-acoustic pulsation. Finally, the fact that peak concentration of flame-kernel events consistently appears approximately 20mm downstream of the nozzle is explained by the fact that shear-layer vortices grow with downstream distance. In the near-nozzle regions, they have yet not reached sufficient size to induce significant flame-surface wrinkling or breakup.

Taken together, the data from the DS- and TM-Burners indicate auto-ignition is not the dominant mechanism responsible for the flame-kernel events observed in the highspeed OH-PLIF data. Although the data does not exclude the possibility that some flame-kernels result from auto-ignition, the majority of flame-kernel events occur in regions of the flow highly non-conducive to auto-ignition. Were auto-ignition the dominant mechanism responsible for the observed flame-kernel events, one would expect a greater concentration of them in regions of the flow more conducive to the phenomenon, such as at the core of the PVC, where strain-rates are lower and residence times are longer. The concentration of flame-kernel events peaks in all cases at the interface between the dominant vortex structure (the PVC in two cases, the shear-layer vortices in the third) and the shear-layer indicates the mechanism responsible is wrinkling and break-up of the primary flame sheet in the combustor. In this mechanism, the sudden appearance of flame-kernels in the PLIF

images is explained by through-plane transport of the highly-wrinkled or fragmented flame sheet.

Conclusion

Long-duration, kHz-framerate OH-PLIF measurements were analyzed to determine the physical mechanism responsible for a previously observed phenomenon wherein isolated pockets of high OH-concentration fluid suddenly appear in regions of unburned gas away from the contiguous flame zone in a gas turbine model combustor. Prior research on the burners indicate these isolated flame-kernels may result either from auto-ignition of hot, unburned reactants upstream of the primary flame or from transport of reacting fluid into the field of view from beyond the imaging plane. An image-processing routine was developed to autonomously identify and statistically characterize these flame-kernels. Phase sorting of the kernel centroids with respect to the dominant fluid-dynamic structure of the combustors (a helical precessing vortex core or thermo-acoustically forced shear-layer vortices) indicate through-plane transport of reacting fluid best explains their sudden appearance the PLIF images.

The concentration of flame-kernel events around the periphery of the mean location of the precessing vortex core (PVC) indicates they are likely the result of wrinkling and break-up of the primary flame sheet associated with the passage of the PVC as it circumscribes the burner centerline. The prevailing through-plane velocity of the swirling flow-field transports these fragments into the imaging plane of the OH-PLIF system. The lack of flame-kernel events near the center of the PVC, where conditions are more conducive to auto-ignition (lower strain, longer fluid dynamic residence time), indicates auto-ignition is not a viable explanation for these flame-kernels in a majority of cases. The lack of flame-kernel centroid variation in the case of the TM-Burner ‘Quiet flame’ (which has no PVC) further supports this explanation.

References

R. Barlow. Proc. Comb. Inst. (2007), 49-75.

B. Böhm, I. Boxx, C. Kittler, W. Meier, A. Dreizler. Proc. Combust. Inst. 32 (2009) 1647–1654

Boxx I, Heeger C, Gordon R, Böhm B, Dreizler A, Meier W (2009b) Combust. Flame, 156:269-271.

I. Boxx, M. Stöhr, C. Carter, W. Meier. Applied Physics B, 95(1) 2009a. 23-29.

I. Boxx, M. Stöhr, C. Carter, W. Meier. Combustion and Flame 157(8) (2010a) 1510-1525. doi: 10.1016/j.combustflame.2009.12.015.

I. Boxx, C. Arndt, C. Carter, W. Meier. Experiments in Fluids, 2010b. (In Press). DOI: 10.1007/s00348-010-1022-x

S. Correa. Proc. Comb. Inst. (1998) 1793-1807.

X. R. Duan, W. Meier, P. Weigand, B. Lehmann, Appl. Phys. B 80 (2005) 389-396.

R. Giezendanner-Thoben, O. Keck, P. Weigand, W. Meier, U. Meier, W. Stricker, M. Aigner, Combust. Sci. Tech. 175 (2003) 721-741.

R. Giezendanner-Thoben, P. Weigand, X. R. Duan, W. Meier, U. Meier, M. Aigner, B. Lehmann, J. Eng. Gas Turb. Power. 127 (2005a) 492-496.

R. Giezendanner-Thoben, U. Meier, W. Meier, M. Aigner. Flow Turb. Combust. 75 (2005b) 317-333.

R. Giezendanner-Thoben, U. Meier, W. Meier, J. Heinze, M. Aigner, Appl. Opt. 44 (2005c) 6565-6577

A.H. Lefebvre, Gas Turbine Combustion, Taylor & Francis, Philadelphia, 1999.

W. Meier, P. Weigand, XR Duan, R. Giezendanner-Thoben. (2007) Combust. Flame 150:2-26. doi.org/10.1016/j.combustflame.2007.04.002

R. Sadanandan, M. Stöhr, W. Meier. Appl. Phys. B 90 (2008) 609-618

A. M. Steinberg, I. Boxx, C. Arndt, J. Frank, W. Meier. Proc. Combust. Inst. 33 (2011) 1663-1672.

A. Steinberg, I. Boxx. M. Stöhr, C. Arndt, W. Meier, C. Carter. AIAA-2011-5554. 47th AIAA/ASME/SAE/ASEE Joint Propulsion Conference and Exhibit, San Diego, California, July 31-3, 2011

M. Stöhr, I. Boxx, C. Carter, W. Meier. Proc. Combust. Inst. 33 (2011) 2953-2960.

P. Weigand, W. Meier, X. R. Duan, W. Stricker, M. Aigner. Combust. Flame 144 (2006) 205-224.

Figures

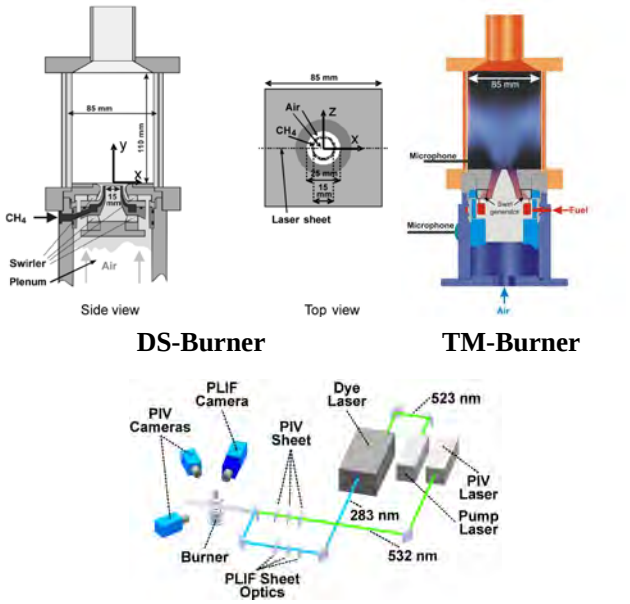

Figure 1 – Burners and experiment configuration.

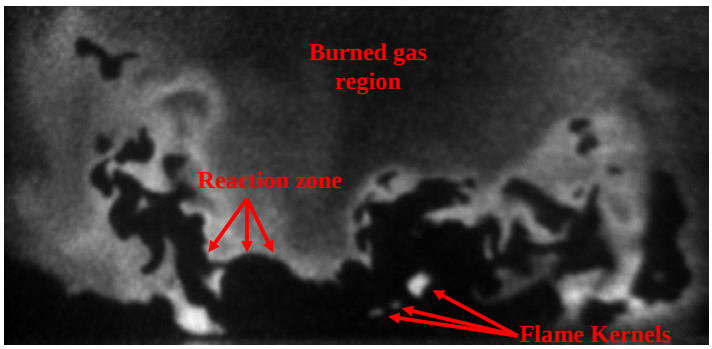

Figure 2 – OH-PLIF Image.

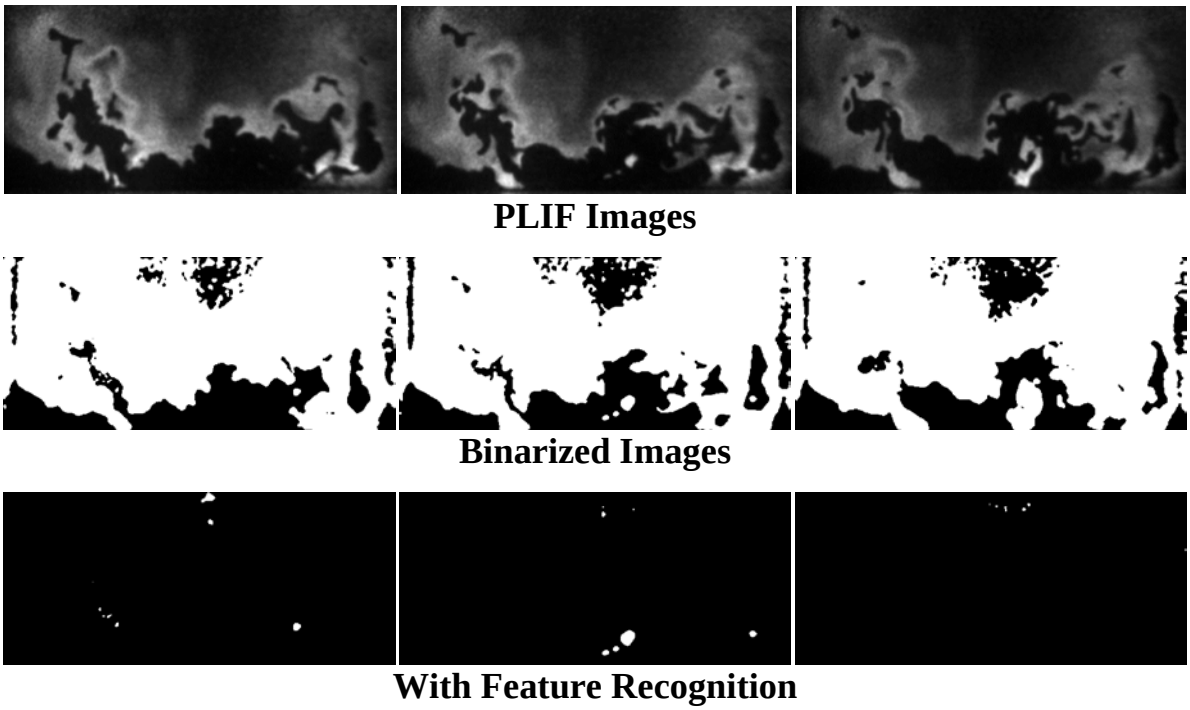

Figure 3 – Steps in the flame-kernel event identification algorithm.

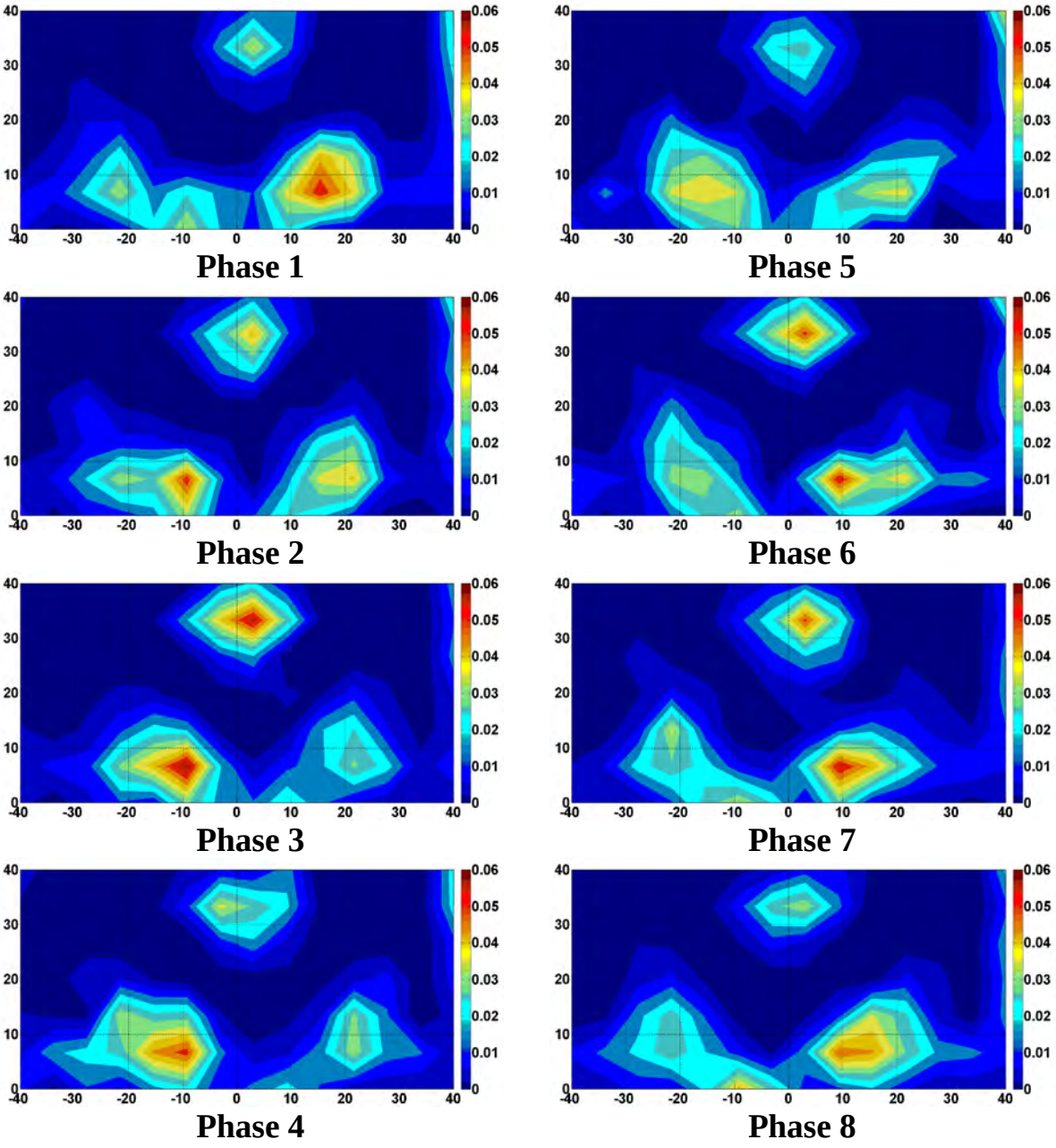

Figure 4 – Phase-sorted, 2D PDF of flame-kernel events in the DS-Burner.

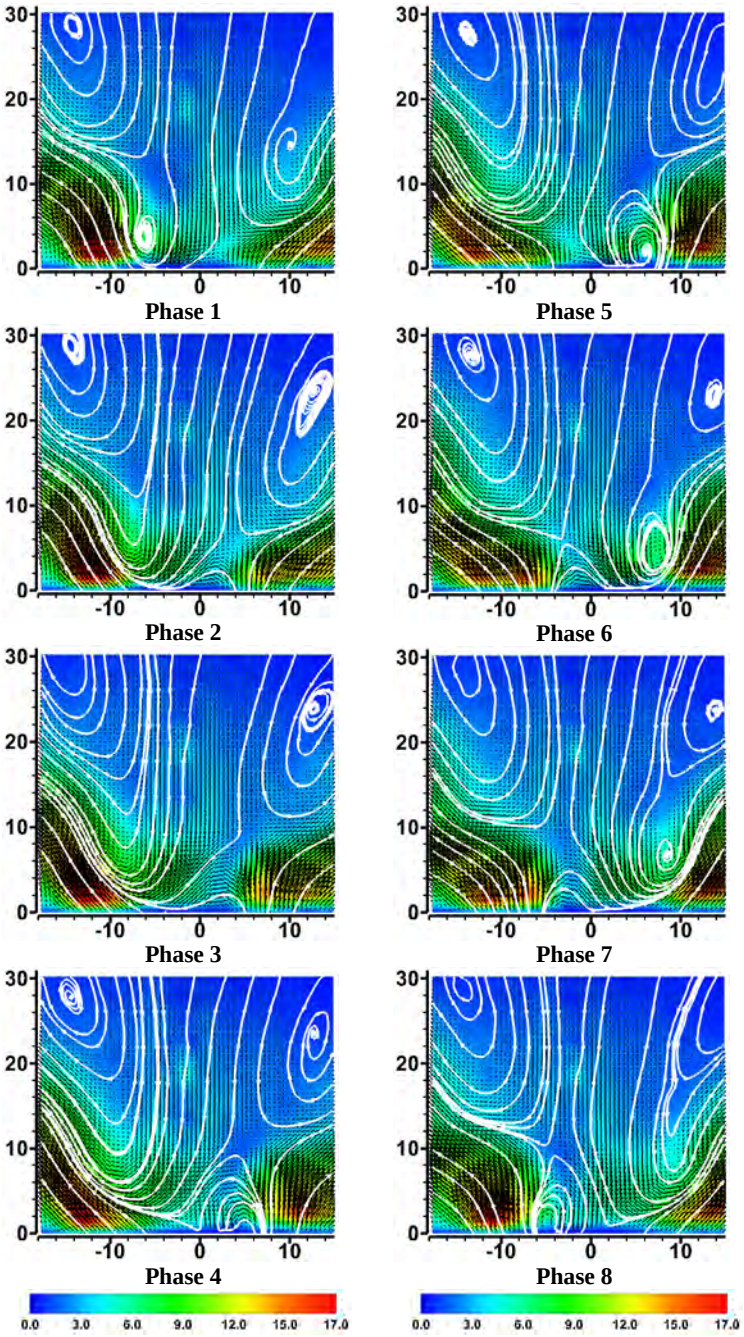

Figure 5 - Phase-averaged velocity magnitude distribution in the DS-Burner. Color contours represent the velocity magnitude, in m/s.

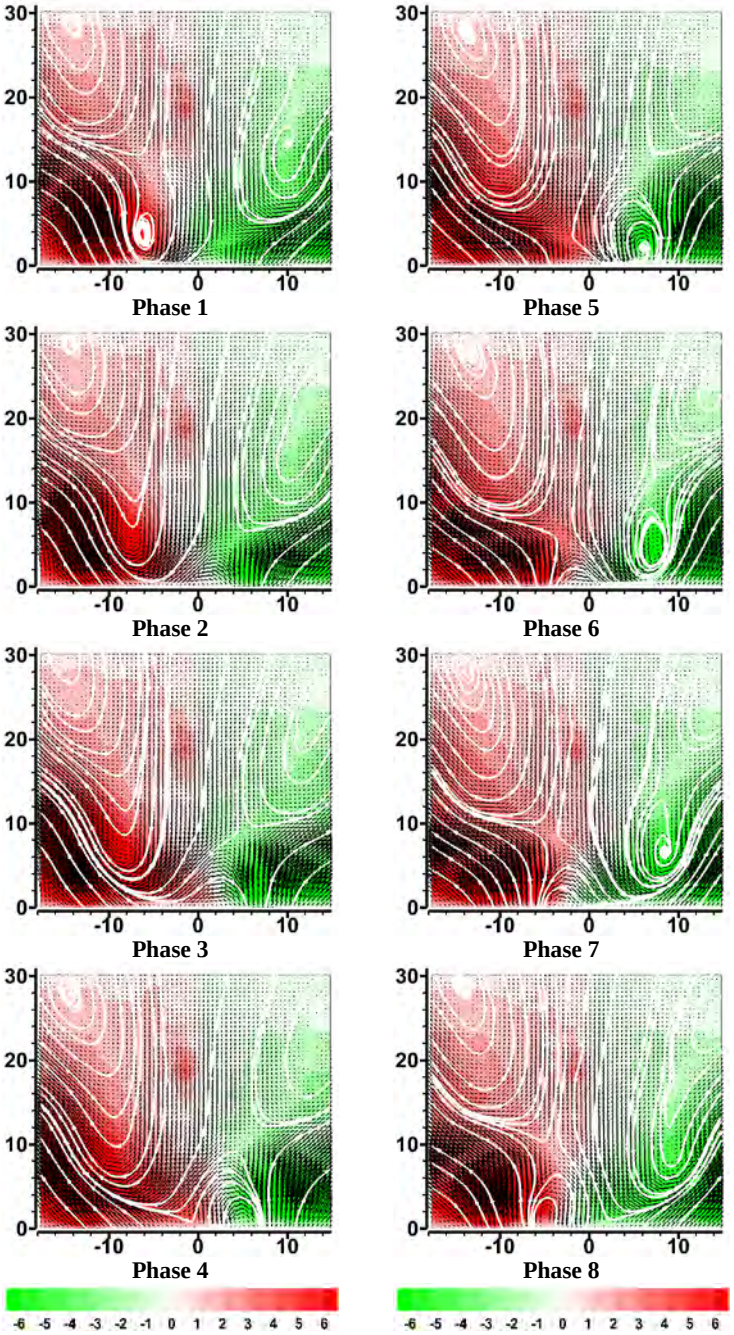

Figure 6 – Phase-averaged through-plane velocity in the DS-Burner. Color contours represent the through-plane component of velocity, Vz, in m/s.

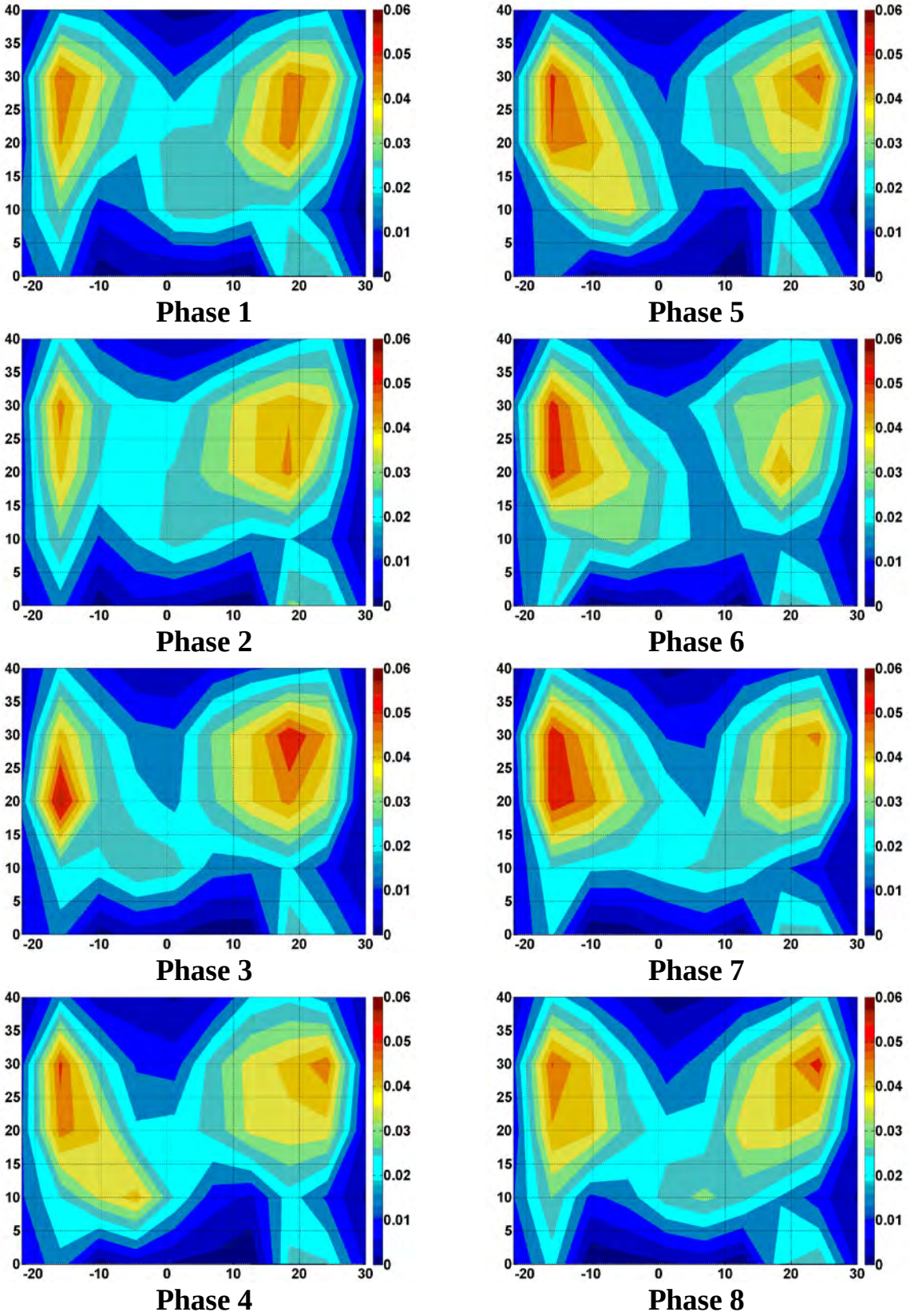

Figure 7 – Phase-sorted probability distribution of flame-kernel events in the 'Noisy Flame' case studied in the TM-Burner. Note, unlike in the DS-Burner, the measurement zone does not span the entire width of the combustor.

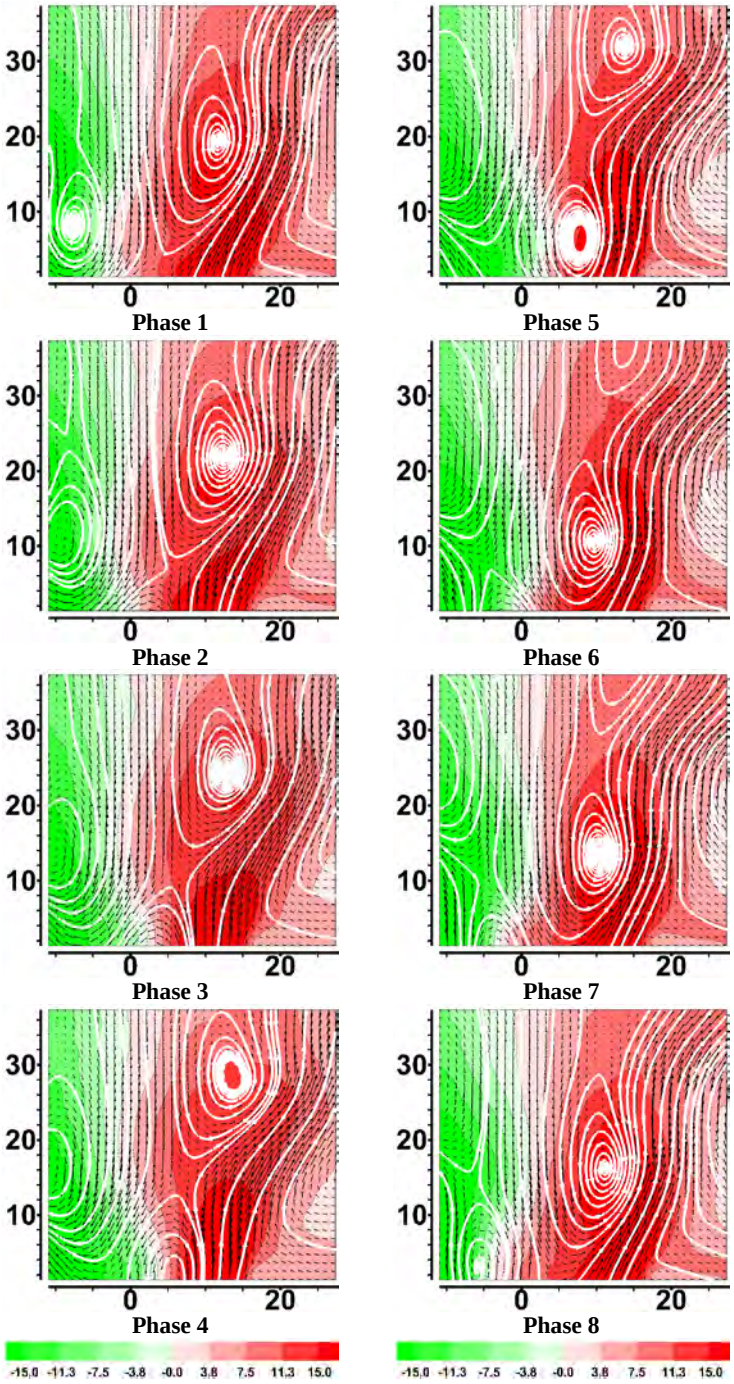

Figure 8 – Phase averaged velocity field measured in the 'Noisy flame' case of the TM-Burner. Color contours represent the through-plane component of velocity, Vz, in m/s.

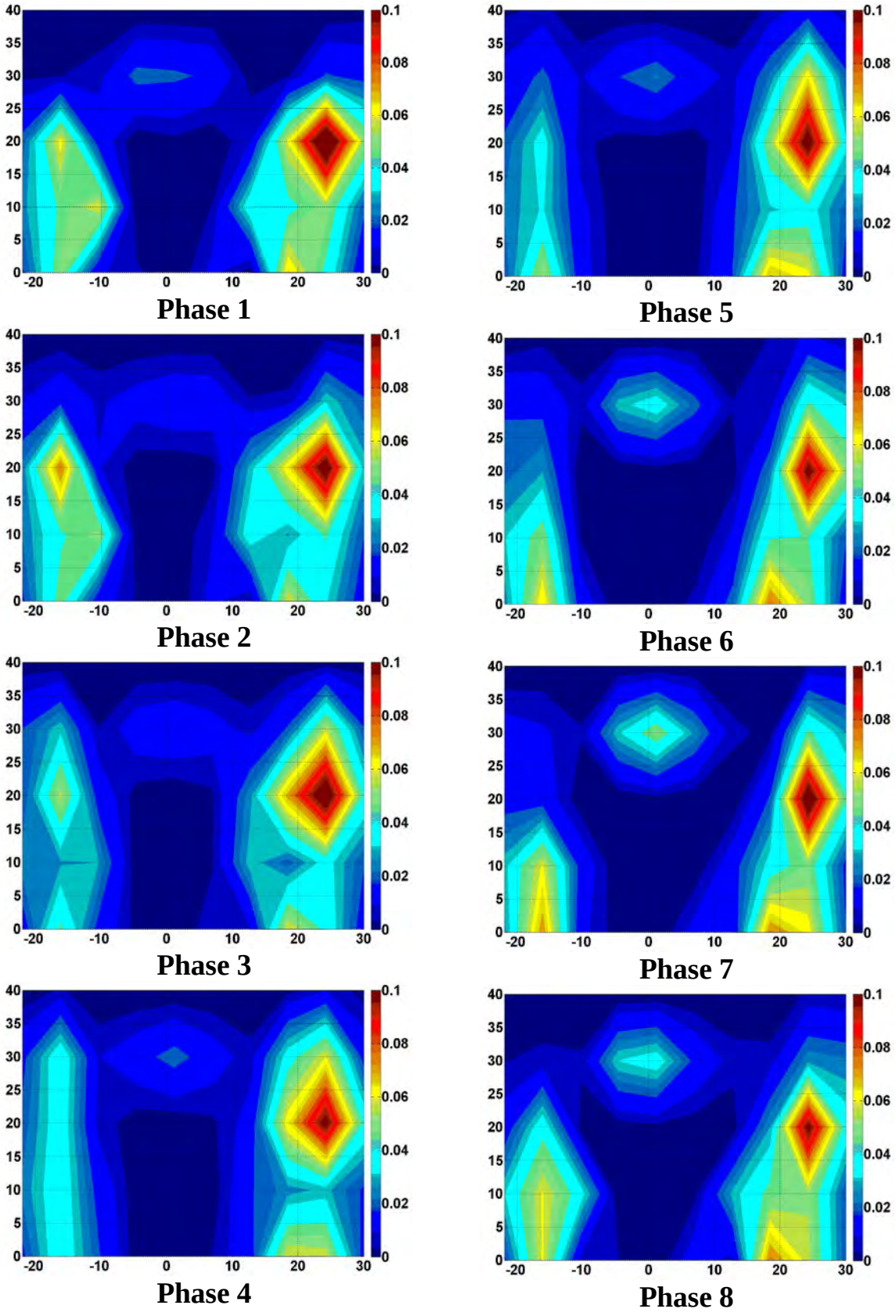

Figure 9 – Spatial distribution of flame kernel events, phase-sorted accord to the dominant velocity eigenmode, for the ‘Quiet flame‘ case studied in the TM-Burner.

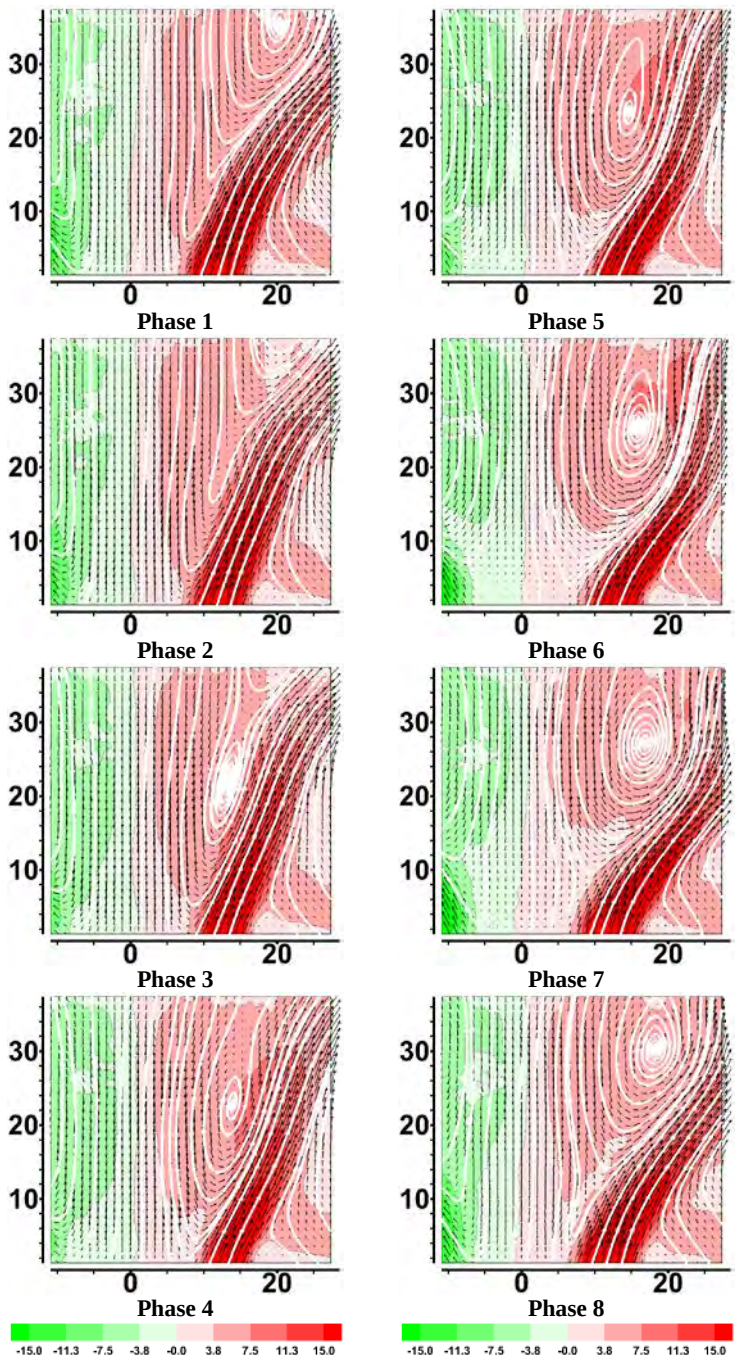

Figure 10 – Phase averaged velocity field measured in the ‘Quiet flame’ case of the TM-Burner. Color contours represent the through-plane component of velocity, Vz, in m/s.